Heliconical magnetic order and field-induced multiferroicity of the Co_2Y-type hexaferrite $Ba_{0.3}Sr_{1.7}Co_2Fe_{12}O_{22}$

Hak Bong Lee
Department of Physics, Korea University, Seoul 136-713, South Korea

Sae Hwan Chun, Kwang Woo Shin, Byung-Gu Jeon, Yi Sheng Chai, and Kee Hoon Kim*
CeNSCMR, Department of Physics and Astronomy, Seoul National University, Seoul 151-747, South Korea

Jürg Schefer
Laboratory for Neutron Scattering, Paul Scherrer Institut, CH-5232 Villigen PSI, Switzerland

Hun Chang, Sae-Na Yun, Tae-Young Joung, and Jae-Ho Chung†
Department of Physics, Korea University, Seoul 136-713, South Korea
(Received 13 August 2012; published 27 September 2012)

Using magnetoelectric measurements and neutron diffraction, we investigated multiferroic properties of Co_2Y hexaferrite $Ba_{0.3}Sr_{1.7}Co_2Fe_{12}O_{22}$ in zero and finite magnetic field ($H \perp c$). Upon zero-field cooling, a longitudinal heliconical magnetic structure was observed below 280 K, which involves incommensurate planar helical ordering. When the magnetic field was applied perpendicular to its c axis, electric polarization was observed and the incommensurate ordering was replaced by a commensurate one as commonly observed in other hexaferrites. Electric polarization remained at its maximum during field reversal at 10 K, which indicates that magnetic anisotropy within the basal planes stabilizes the field-induced electric polarization.

DOI: 10.1103/PhysRevB.86.094435 PACS number(s): 75.85.+t, 75.25.−j, 75.30.Gw, 75.50.Gg

I. INTRODUCTION

Complex interplay between multiple order parameters is one of the central issues in the current condensed-matter research. Strong cross couplings between magnetic and electronic order parameters may produce novel functionalities that enable manipulation of magnetic order using electric field, or of electronic order using magnetic field.[1–4] Such magnetoelectric coupling can be found in antiferromagnets lacking spatial magnetic inversion symmetry, which can in turn lead to breaking of lattice inversion symmetry.[5–7] Since magnetic energies are typically weaker than lattice energies, these phenomena are usually observed at cryogenic temperatures.[8–12] In order to realize useful devices that exploit these novel phenomena, the coupling should be stable enough to appear at room temperature yet flexible enough to be controllable at low fields.

Magnetoelectric couplings robust at room temperature (RT) are often observed in antiferromagnets involving strong superexchange interactions between Fe^{3+} ($3d^5$) ions. Ferrites with hexagonal (or rhombohedral) symmetry are good examples, which include $BiFeO_3$[13,14] and various hexaferrites.[4,15–20] $BiFeO_3$ exhibit ferroelectric and antiferromagnetic transitions well above RT ($T_C \sim 1100$ K and $T_N \sim 643$ K), which is a key reason for a large amount of research efforts given to it. Albeit its simple crystal structure, the intrinsic properties are difficult to achieve and only recently being uncovered.[14] In contrast, hexaferrites have long been used for industrial applications, and include a large family of structural variants that allow a wide range of physical parameters.[21] They typically have long-range commensurate ferrimagnetic (FIM) orderings well above RT, but occasionally exhibit noncollinear incommensurate orderings at low temperatures. However, electric polarization is not observed in zero field because proper-screw helices, typical of hexaferrites with noncollinear order, do not produce spin-current polarization.[5] The initial discovery of magnetoelectricity in a Y-type $Ba_{0.5}Sr_{1.5}Zn_2Fe_{12}O_{22}$ (Zn_2Y or BSZFO) required an external magnetic field ($\gtrsim$0.2 T) perpendicular to the c axis, because significant easy-plane anisotropy must be overcome.[15,22]

The magnetoelectric properties of hexaferrites can be modified by substituting magnetic or nonmagnetic ions and thereby adjusting lattice. For instance, helical pitches of incommensurate order can be controlled by compositions of alkaline earth ions[22,23] or replacing Fe^{3+} ions.[24,25] Once helical order is established, magnetoelectric susceptibility can greatly be enhanced, for example, by substituting Al into BSZFO.[16] $Ba_2Mg_2Fe_{12}O_{22}$ (Mg_2Y or BMFO) also shows electric polarization at low fields.[17] The origin of the enhanced susceptibilities is ascribed to the appearance of heliconical magnetic order due to partial replacement of Fe^{3+} ions and subsequent reduction of magnetic anisotropy.[16,17,26,27] [See Fig. 1(a) for their structural lattice and Fig. 1(b) for schematics of the associated spin structures.[28]] Explicit observations of electric polarization at RT have recently been realized in cobalt-containing Z-type hexaferrites.[4,19] Since Co^{2+} ($3d^7$) ions are also magnetic contrary to Mg^{2+} or Al^{3+}, it is supposed that they contribute to enhancing magnetic ordering temperatures.

In this work, we report the field-induced electric polarization and magnetic phase transitions in Co_2Y-type hexaferrite $Ba_{0.3}Sr_{1.7}Co_2Fe_{12}O_{22}$ (BSCFO). Heliconical structures appeared near RT, and electric polarization was induced in the same phase at low temperatures. Whereas the field response overall was similar to the case of Al-doped BSZFO,[16,26] we observed a distinctive plateau in the electric polarization

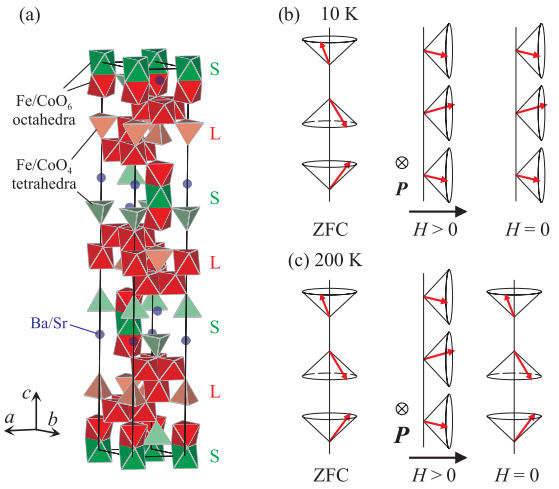

FIG. 1. (Color online) (a) Crystal structure of the Y-type hexaferrite. The green and red polygons represent S and L blocks, respectively, according to Ref. 23. Shown in the right panel are schematic illustrations of the magnetic structures of BSCFO in zero-field cooling (ZFC), under finite field ($H \perp c$), and subsequently in zero field at (b) 10 K and (c) 200 K.[28] Only the net spin vectors of L blocks are shown for simplicity. Note that the spiral pitch is incommensurate to the lattice for the longitudinal cones but commensurate for the transverse. Arrows indicate the direction of the field, and **P** represents the observed electric polarization.

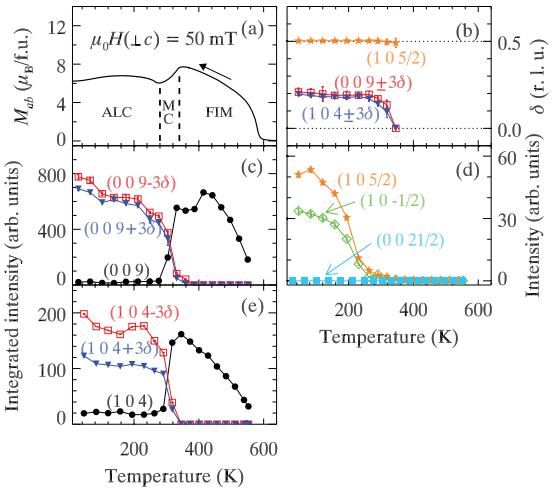

FIG. 2. (Color online) Temperature dependencies of (a) the low-field magnetization ($M_{ab} \perp c$), (b) the incommensurability, δ, and (c)–(e) the integrated intensities of magnetic Bragg peaks. ALC, MC, and FIM are short for alternating longitudinal conical, mixed conical, and ferrimagnetic phases, respectively. The solid lines in (b)–(e) are guides to the eye.

during field reversal 10 K. This behavior suggests that there are additional magnetic anisotropy terms within a-b planes stabilizing magnetization as well as electric polarization in zero field.

II. EXPERIMENTAL

Single crystalline samples were grown from Na_2O-Fe_2O_3 flux in air following the process described in Ref. 4. The crystal structure of the obtained Co_2Y crystals belongs to the $R\bar{3}m$ space group with lattice parameters $a = 5.8601$ Å and $c = 43.4211$ Å, which were confirmed by neutron diffraction. For dc magnetization, dielectric constant, and electric polarization measurements, crystals were cooled in zero field down to the base temperature, and magnetic field was then applied perpendicular to the c axis. Electric polarization ($P \perp H$ & $P \perp c$) was obtained by integrating magnetoelectric current measured under applied electric field ($E = +330$ kV/m). An *LCR* meter was used for dielectric constant ε measurements at 7.5 MHz.

Neutron-diffraction measurements were performed using two instruments. Temperature dependence in zero field was measured using the BT9 triple-axis spectrometer ($\lambda = 2.41$ Å) of the NIST Center for Neutron Research. Pyrolitic graphite filters were used in order to remove higher order contaminations. Field dependence ($H \perp c$) was measured using the TriCS four-circle diffractometer[29] at Swiss Spallation Source (SINQ)[30] of the Paul Scherrer Institute [$\lambda = 2.32(1)$ Å]. Two-axis mode was used with the crystal oriented on the $h0l$ scattering plane inside the superconducting split-pair cryomagnet, so that the magnetic field was applied parallel to the b axis.

III. RESULTS AND DISCUSSIONS

A. Magnetic ordering in zero field

Temperature dependence of the low-field dc magnetization, M_{ab} ($\perp c$) plotted in Fig. 2(a), shows that long-range magnetic order in BSCFO appears well above RT. An initial large increase observed at $T_N \approx 580$ K corresponds to the onset of FIM ordering, which is a typical high-temperature phase of Y-type hexaferrites.[22,27,31] Upon further cooling two anomalies were observed at ~280 and 340 K, respectively, which suggested there are additional magnetic phase transitions above and near RT. The nature of these phases could be revealed by using the neutron-diffraction method. Plotted in Fig. 3 are the neutron-diffraction intensities observed along [0 0 l] and [1 0 l] directions of BSCFO at selected temperatures. Broad incommensurate peaks are clearly visible over a wide temperature range near wave vectors $\mathbf{Q} = \mathbf{Q}_N \pm \mathbf{k}_2 = \mathbf{Q}_N \pm 3(0,0,\delta)$, where $\delta \approx 0.2$. (Note that the nuclear Bragg peaks, $\mathbf{Q}_N$, should satisfy the reflection condition $-h + k + l = 3n$.) It indicates that planar helical order exists in BSCFO similarly to Zn_2Y or Mg_2Y, suggesting the possibility of magnetoelectricity under external magnetic field. At low temperatures, we also observed resolution-limited peaks at $\mathbf{Q} = \mathbf{Q}_N \pm \mathbf{k}_1 = \mathbf{Q}_N \pm 3(0,0,0.5)$ along [1 0 l] directions. [See Fig. 3(b).] These peaks were invisible along [0 0 l], indicating that the associated spin components are parallel to the c axis. [See Fig. 3(a).] The combination of these two types of order accounts for the so-called alternating longitudinal conical (ALC) phase previously observed in Al-doped BSZFO.[26,27] [See Fig. 1(b) for the schematics of the ALC structure.] As the temperature was raised, the $\mathbf{k}_1$ peaks disappeared near RT, whereas the $\mathbf{k}_2$ peaks also became weaker and moved closer to nuclear Bragg peaks. This indicates that the spin structure became more planar while the spiral pitch is reduced at higher temperatures. The nuclear peak intensities, at the same time, enhanced greatly in both scans above RT. Such change is consistent with the appearance

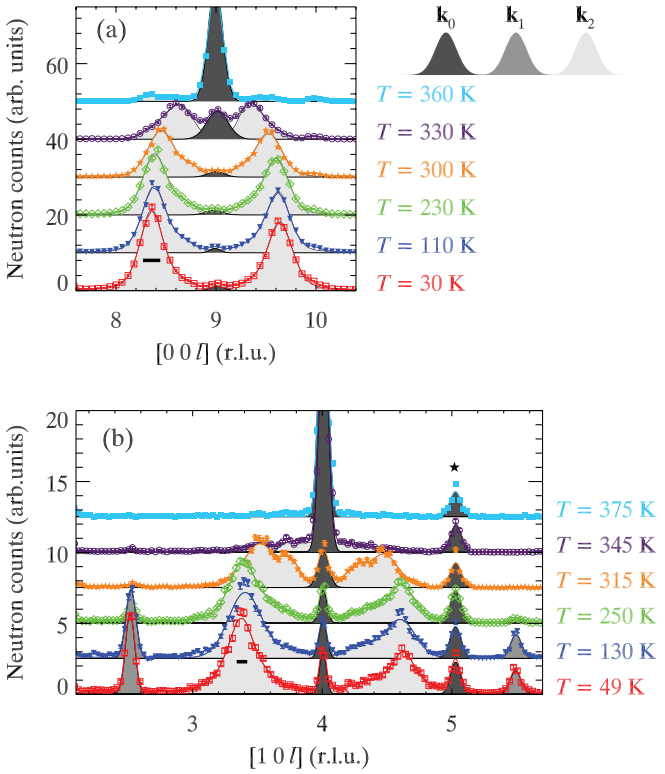

FIG. 3. (Color online) Temperature dependence of the neutron-diffraction intensities in zero-field cooling. Gray areas of different shades represent Gaussian-fitted Bragg peaks that belong to different propagation vectors: $\mathbf{k}_0$, $\mathbf{k}_1$, and $\mathbf{k}_2$, respectively, in the order of decreasing shades. Thin solid lines are Gaussian fits to the data. Thick horizontal bars mark estimated instrumental resolution. The star symbol indicates the peak ascribed to the twinned domain.

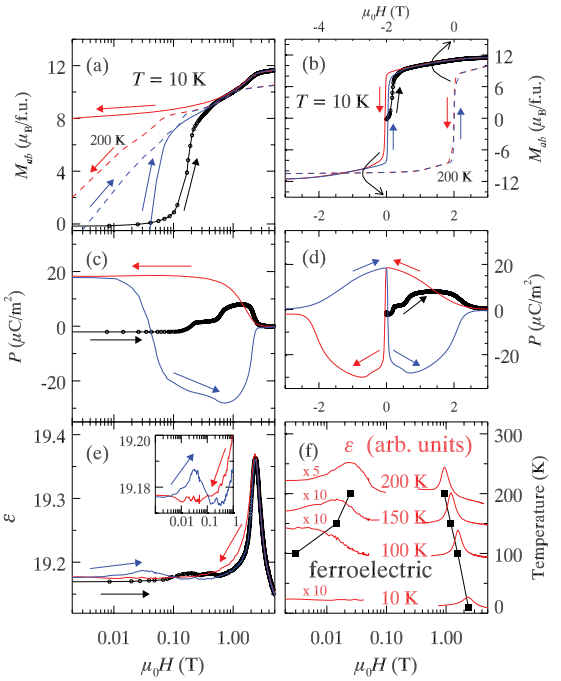

FIG. 4. (Color online) Magnetic-field dependencies of (a) and (b) dc magnetization, (c) and (d) electric polarization, and (e) dielectric constant. The data were measured at 10 K, except those of dashed lines measured were at 200 K. In all plots, black open circles mark the data during initial magnetization processes after zero-field cooling, whereas red and blue lines correspond to field-down and field-up processes, respectively, as indicated by arrows. Note that the plots in (b) are shifted horizontally for clarity. The magnetoelectric phase diagram is summarized in (f). Superimposed on the phase diagram using red solid lines are the dielectric curves at selected temperatures.

of FIM order, $\mathbf{k}_0$ = (0, 0, 0), suggested in the magnetization data.

We have extracted the temperature dependencies of the neutron-scattering data and summarized them in Figs. 2(b)–2(e). It is shown that the incommensurate $\mathbf{k}_2$ peaks are observed up to ∼340 K, whereas the commensurate $\mathbf{k}_1$ peaks seem to get suppressed earlier but still persist up to the same temperature. Between 280 and 340 K, where the two anomalies were observed in the magnetization, we notice that all three of $\mathbf{k}_0$, $\mathbf{k}_1$, and $\mathbf{k}_2$ peaks more or less coexist. We refer to this temperature range as mixed conical (MC). Beyond 340 K, only the $\mathbf{k}_0$ peaks are observed. From these results we may summarize that the magnetic ordering of BSCFO in zero field is similar to BMFO[32] or Al-doped BSZFO[27] in general, but the ALC phase extends down to 10 K with apparent absence of the normal (nonalternating) longitudinal conical phase.

Note that the $\mathbf{k}_2$ peaks in BSCFO are very broad and could not be reasonably fitted either by the single Gaussian or Lorentzian function. This seems to suggest that the magnetic correlation along the c axis is particularly short, and not more than four times the c-axis parameter. Their anomalous widths are more apparent in [1 0 l] scans [Fig. 3(b)] measured under a high-resolution setup. In some scans, it was even suggestive of separations into multiple phases with different incommensurate propagation vectors. Since we could not clearly separate them, we used double pseudo-Voigt functions only for the purpose of fitting and plotted their weighted averages in Fig. 2(b) or summations in Figs. 2(c)–2(e).

B. Field-induced electric polarization

External magnetic field was applied perpendicular to the c axis in order to observe changes in magnetic and magnetoelectric properties. The field-dependent magnetization curves revealed a few notable behaviors. First, M_{ab} remained suppressed when the field was applied immediately following zero-field cooling, and merged to the main loops at relatively high fields (≳100 mT). [See Figs. 4(a) and 4(b).] Similar behaviors have already been observed in other Y-type hexaferrites, and suggest that the zero-field magnetic structures are different between before and after application of external magnetic field. Second, the main loops exhibited ferromagnetic hysteresis at 10 K, in which M_{ab} remained nearly constant below 0.1 T. Reversal of the magnetization was observed at the coercive field of ∼40 mT. Such hard-ferromagnetic behavior is in a clear contrast to other hexaferrites, in which M_{ab} largely diminishes near zero field,[4,18,19,26,31] and suggests there is a significant pinning field stabilizing the magnetization. Even at 200 K where coercivity becomes negligible, the slope of $M_{ab}(\mu_0 H)$ curves still remained very large.

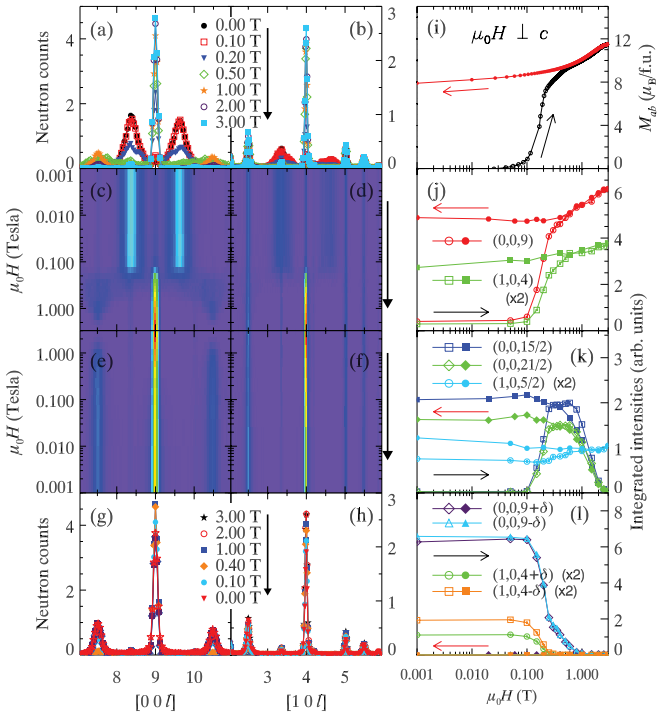

FIG. 5. (Color online) (a)–(h) Field dependence ($H \perp c$) of the neutron-scattering intensities at 10 K. The arrows indicate the directions of the changes in field. (i) Initial and down-field magnetization measured by vibrating sample magnetometry. (j)–(l) Summary of the field dependence of the Bragg peak intensities at 10 K. Arrows indicate directions of field change.

Above features in the magnetization curves are directly related to the magnetoelectric behaviors, which are shown in Figs. 4(c)–4(e). The magnetoelectric polarization remained negligible during initial magnetization, which started to increase coincidentally at the upturn of the magnetization curve. A sharp peak in dielectric constant as well as a drop in electric polarization were observed at high field where the magnetization curve entered the plateau region. During the field-down process, we observed that the polarization was regained and remained constant down to zero field once it reached the maximum below 100 mT at 10 K. A negative coercive field was required to reverse the electric polarization, which is simultaneously indicated by a small peak in the dielectric constant. [See the inset of Fig. 4(c).] The constant polarization in low fields is consistent with the magnetization behavior, and indicates that BSCFO is a stable field-induced ferroelectrics at low temperatures. At higher temperatures, such stability was gradually lost and the lower limits of the polarization appeared at positive fields. Our magnetoelectric measurements were limited up to 200 K due to high leakage current. The obtained magnetoelectric phase diagram is summarized in Fig. 4(f), which is qualitatively similar to that of Al-doped BSZFO.[16]

C. Magnetic ordering under external field

We then performed neutron-diffraction measurements in order to understand magnetic order in the field-induced phases. The results at 10 K are summarized in Fig. 5. The left panel of Fig. 5 explicitly shows the field-dependent changes of the Bragg peaks. When the field was increased following zero-field cooling, the $\mathbf{k}_2$ peaks disappeared near 0.1 T. [See Figs. 5(a)–5(d).] At the same time, intensities of the $\mathbf{k}_1$ and the nuclear peaks ($\mathbf{k}_0$) sharply increased simultaneously. It is notable that intense new peaks appeared at wave vectors corresponding to $\mathbf{k}_1$ along [0 0 l], where the peaks had been invisible in zero-field cooling. This indicates that the associated spin components are no longer parallel to the c axis. These changes are similar to the case of Al-doped BSZFO[26] and indicate that transverse commensurate conical structure is established in the field.[32] [See the middle ($H > 0$) of Fig. 1(b) for the schematics of the transverse structure.] Upon further increase of the field beyond 1 T where electric polarization had been suppressed [Fig. 4(d)], the $\mathbf{k}_1$ peaks along [0 0 l] eventually disappeared whereas the $\mathbf{k}_0$ peaks continued to be enhanced. All these field dependent behaviors are consistent with the initial magnetization data shown in Fig. 5(i).

The data during ramping the field down are also consistent with the magnetization. [See Figs. 5(e)–5(h).] When the field was reduced below 1 T, the intensities of $\mathbf{k}_0$ or $\mathbf{k}_1$ peaks were recovered. Upon further reduction of the field, however, the initial intensities did not reappear and all the peak intensities remained nearly constant below 0.1 T down to zero field. Most notably, the $\mathbf{k}_2$ peaks did not reappear at all. This behavior indicates that the field-induced structure is not only different from zero-field-cooling structure, but also becomes locked in at low fields. The reversal of the FIM domains near the negative coercive field was also observable as an increase of diffuse scattering intensities (not shown).

Two coexisting magnetic anisotropy fields were previously identified to be responsible for heliconical order in Y-type hexaferrites, which are easy-axis and easy-plane with respect to the c axis of the hexagonal lattice.[27] Since the spins will rotate along constant-energy paths during magnetization reversal, reductions of the polarization in BSZFO and BMFO can be understood as magnetic domain formation by rotating about the c axis. In contrast, the constant magnetization and polarization in BSCFO strongly suggest that such rotations do not occur readily near zero field. Therefore, we conclude that Co^{2+} ions contribute to additional anisotropy terms, as functions of angle about the c axis, which can stabilize magnetization and electric polarization. The magnitude of such anisotropy field at 10 K can be estimated by the negative coercivity, ~40 mT. This anisotropy term in the basal planes of hexaferrites corresponds to the third term of the anisotropy energy equation: $F_K = K_1 \sin^2\theta + K_2 \sin^4\theta + K_3 \sin^6\theta \cos 6\varphi$, in which θ and φ are polar angles with respect to the c axis.[33] The six-fold symmetry of its φ dependence has already been observed in Co_2Y and $Co_{1.5}Fe_{0.5}Z$ hexaferrites.[21] The coercivity observed in our sample is comparable to the anisotropy field (~340 Oe at 100 K) reported in the early work. The suspected multiple $\mathbf{k}_2$ peaks appearing near RT [Fig. 3(b)] may also be explained by this in-plane term because it will certainly prevent the spiral pitch from changing continuously as a function of temperature.

When the temperature was raised in zero field after the sample had been exposed to external field, the $\mathbf{k}_2$ peaks slowly reappeared and the $\mathbf{k}_1$ peaks disappeared. [See Fig. 6(a).] It

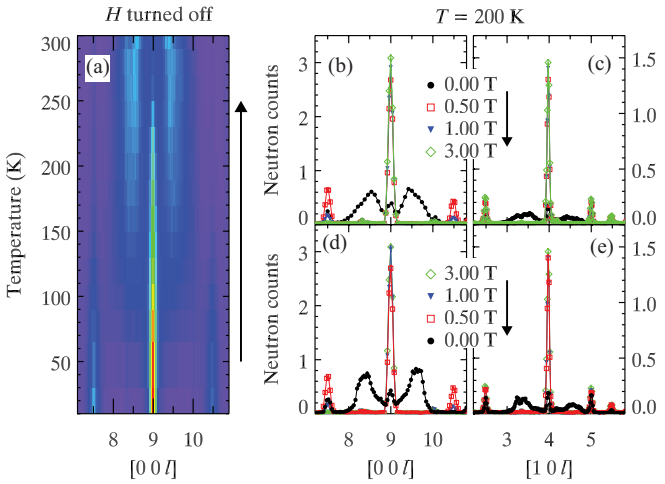

FIG. 6. (Color online) (a) 2D plot of the temperature dependence of the Bragg peak intensities in zero field after the crystal was exposed to $\mu_0 H(\perp c) = 3.0$ T at 10 K. The data were measured during the temperature increase as indicated by the arrow. (b)–(e) Field dependence of the Bragg peak intensities at 200 K. The arrows indicate the directions of the changes in field.

shows that the locked-in commensurate order overcomes the major anisotropy field by thermal fluctuations. When the field cycling experiment was performed at 200 K, where electric polarization disappeared in zero field, the incommensurate ALC phase was almost fully recovered. [See Figs. 6(b)–6(e).] It can thus be consistently understood according to the spin-current mechanism that the finite electric polarization is observed only when the axis of spin cone is not parallel to the spin propagation direction.[5,26] The schematics of the field-dependent magnetic structures are compared between 10 and 200 K in Figs. 1(b) and 1(c). All these data confirm that the field-induced magnetoelectricity of BSCFO is directly related to the underlying magnetic order.

IV. SUMMARY AND CONCLUSION

In summary, we have investigated the magnetoelectric properties and magnetic order of single-crystal BSCFO in zero and finite external magnetic field [$\mu_0 H(\perp c) = 0$–3 T]. In zero field below RT, the ground-state magnetic structure was found to be the alternating longitudinal heliconical type. Electric polarization was successfully induced when external magnetic field was applied perpendicular to the c axis, and the helicones in this field range were transverse and commensurate. Whereas the overall field dependence was similar to Al-doped Zn_2Y hexaferrites, the constant magnetization and electric polarization near field reversal revealed a pinning force due to an additional anisotropy term within the basal a-b planes.

The results presented in this work add to the list of magnetoelectric hexaferrites, in which electric polarization is induced when external magnetic fields transform heliconical spin structures into transverse commensurate. This corroborates the idea that the magnetoelectric properties of various hexaferrites can be explained within a single picture that includes coexisting easy-plane and easy-axis anisotropy fields. Furthermore, the current results observed in BSCFO provide a unique possibility that cobalt ions can play an effective role in stabilizing ferroelectric polarization of hexaferrites.

ACKNOWLEDGMENTS

This work is based on experiments performed at the Swiss spallation neutron source SINQ (TriCS), Paul Scherrer Institute, Villigen, Switzerland. The authors are also grateful to the NIST Center for Neutron Research for providing neutron-scattering facilities and experimental support. This work is financially supported by National Research Foundation of Korea through the Nuclear Research and Development Program (Grants No. 2011-0031933 and No. 2012-025968) and the Basic Research Program (Grant No. 2012-029621). The work at Seoul National University was supported by National Creative Research Initiatives (Grant No. 2010-0018300).

*khkim@phya.snu.ac.kr
†jaehc@korea.ac.kr

[1] S-W. Cheong and M. Mostovoy, Nat. Mater. **6**, 13 (2007).
[2] D. I. Khomskii, Physics **2**, 20 (2009).
[3] Y. J. Choi, C. L. Zhang, N. Lee, and S-W. Cheong, Phys. Rev. Lett. **105**, 097201 (2010).
[4] S. H. Chun, Y. S. Chai, B.-G. Jeon, H. J. Kim, Y. S. Oh, I. Kim, H. Kim, B. J. Jeon, S. Y. Haam, J.-Y. Park, S. H. Lee, J.-H. Chung, J.-H. Park, and K. H. Kim, Phys. Rev. Lett. **108**, 177201 (2012).
[5] H. Katsura, N. Nagaosa, and A. V. Balatsky, Phys. Rev. Lett. **95**, 057205 (2005).
[6] M. Mostovoy, Phys. Rev. Lett. **96**, 067601 (2006).
[7] A. B. Harris, Phys. Rev. B **76**, 054447 (2007).
[8] N. Hur, S. Park, P. A. Sharma, J. S. Ahn, S. Guha and S-W. Cheong, Nature (London) **429**, 392 (2004).
[9] G. Lawes, A. B. Harris, T. Kimura, N. Rogado, R. J. Cava, A. Aharony, O. Entin-Wohlman, T. Yildrim, M. Kenzelmann, C. Broholm, and A. P. Ramirez, Phys. Rev. Lett. **95**, 087205 (2005).
[10] M. Kenzelmann, A. B. Harris, S. Jonas, C. Broholm, J. Schefer, S. B. Kim, C. L. Zhang, S.-W. Cheong, O. P. Vajk, and J. W. Lynn, Phys. Rev. Lett. **95**, 087206 (2005).
[11] K. Taniguchi, N. Abe, T. Takenobu, Y. Iwasa, and T. Arima, Phys. Rev. Lett. **97**, 097203 (2006).
[12] Y. Yamasaki, S. Miyasaka, Y. Kaneko, J.-P. He, T. Arima, and Y. Tokura, Phys. Rev. Lett. **96**, 207204 (2006).
[13] J. Wang, J. B. Neaton, H. Zheng, V. Nagarajan, S. B. Ogale, B. Liu, D. Viehland, V. Vaithyanathan, D. G. Schlom, U. V. Waghmare, N. A. Spaldin, K. M. Rabe, M. Wuttig, and R. Ramesh, Science **299**, 1719 (2003).
[14] G. Catalan and J. F. Scott, Adv. Mater. **21**, 2463 (2009).
[15] T. Kimura, G. Lawes, and A. P. Ramirez, Phys. Rev. Lett. **94**, 137201 (2005).
[16] S. H. Chun, Y. S. Chai, Y. S. Oh, D. Jaiswal-Nagar, S. Y. Haam, I. Kim, B. Lee, D. H. Nam, K.-T. Ko, J.-H. Park, J.-H. Chung, and K. H. Kim, Phys. Rev. Lett. **104**, 037204 (2010).

[17]S. Ishiwata. Y. Taguchi, H. Murakawa, Y. Onose, and Y. Tokura, Science **319**, 1643 (2008).
[18]Y. Tokunaga, Y. Kaneko, D. Okuyama, S. Ishiwata, T. Arima, S. Wakimoto, K. Kakurai, Y. Taguchi, and Y. Tokura, Phys. Rev. Lett. **105**, 257201 (2010).
[19]Y. Kitagawa, Y. Hiraoka, T. Honda, T. Ishikura, H. Nakamura, and T. Kimura, Nat. Mater. **9**, 797 (2010).
[20]K. Okumura, T. Ishikura, M. Soda, T. Asaka, H. Nakamura, Y. Wakabayashi, and T. Kimura, Appl. Phys. Lett. **98**, 212504 (2011).
[21]J. Smit and H. P. J. Wijn, *Ferrites*, Chap. 9 (Philips Technical Library, Eindhoven, 1959).
[22]N. Momozawa, Y. Yamaguchi, H. Takei, and M. Mita, J. Phys. Soc. Jpn. **54**, 771 (1985).
[23]N. Momozawa, J. Phys. Soc. Jpn. **55**, 4007 (1986).
[24]N. Momozawa, Y. Nagao, S. Utsumi, M. Abe, and Y. Yamaguchi, J. Phys. Soc. Jpn. **70**, 2724 (2001).
[25]O. P. Aleshko-Ozhevskii, R. A. Sizov, I. I. Yamzin, and V. A. Lubimtsev, Sov. Phys. JETP **28**, 425 (1969).
[26]H. B. Lee, Y.-S. Song, J.-H. Chung, S. H. Chun, Y. S. Chai, K. H. Kim, M. Reehuis, K. Prokeš, and S. Mat'aš, Phys. Rev. B **83**, 144425 (2011).
[27]H. Chang, H. B. Lee, Y.-S. Song, J.-H. Chung, S. A. Kim, I. H. Oh, M. Reehuis, and J. Schefer, Phys. Rev. B **85**, 064402 (2012).
[28]In this work, the spin structures of BSCFO were not obtained by the structure refinement method. It is because the long *c*-axis parameter and the small incommensurate propagation vector made it practically impossible to collect a sufficiently large number of Bragg peaks without overlaps. The spin structures shown in Fig. 1 are drawn schematically based on observed propagation vectors and the previous knowledge of the BSZFO structures.[26,27]
[29]J. Schefer, M. Könnecke, A. Murasik, A. Czopnik, Th. Strässle, P. Keller, and N. Schlumpf, Physica B **276-278**, 168 (2000).
[30]W. E. Fischer, Physica B **234-236**, 1202 (1997).
[31]H. Sagayama, K. Taniguchi, N. Abe, T. H. Arima, Y. Nishikawa, S. I. Yano, Y. Kousaka, J. Akimitsu, M. Matsuura, and K. Hirota, Phys. Rev. B **80**, 180419(R) (2009).
[32]S. Ishiwata, D. Okuyama, K. Kakurai, M. Nishi, Y. Taguchi, and Y. Tokura, Phys. Rev. B **81**, 174418 (2010).
[33]J. Smit and H. P. J. Wijn, *Ferrites*, Chap. 4 (Philips Technical Library, Eindhoven, 1959).